A Contactless Electrical Energy Transmission System for Portable-Telephone Battery Chargers

Yungtaek Jang and Milan M. Jovanović

DELTA Products Corporation
Power Electronics Laboratory
P.O. Box 12173, 5101 Davis Drive
Research Triangle Park, NC 27709, USA

Abstract - **A high-performance contactless electrical energy transmission (CEET) technique which employs the inductive energy transmission principle is described. The proposed technique enables the implementation of high-efficiency, high-power-density, fully-regulated CEET systems suitable for applications with a wide input and load range. Specifically, the described CEET system is suitable for the use in universal-input battery chargers.**

1. Introduction

In many applications, the contactless electrical energy transmission (CEET) has distinct advantages over the conventional energy transmission which uses wires and connectors. For example, CEET has been the preferred power-delivery approach in hazardous applications such as mining and underwater environments due to the elimination of the sparking and the risk of electrical shocks [1]. Also, a number of CEET systems have been developed for electric vehicle battery-recharging applications because of their potential enhanced safety, reliability, and convenience. In addition, CEET has been considered in some medical applications since it makes possible to transfer electric energy, which is required for running implanted electrical circulatory assist devices, through the intact skin of a patient [2]. Finally, CEET has been used in cordless electric toothbrushes and portable telephones to increase their reliability by eliminating the contacts between their battery charger and the battery.

Generally, CEET is implemented by using magnetic induction, i.e., by employing specially constructed transformers. In such transformers, the energy from the primary to the secondary is transferred inductively through the air. Because of safety requirements and/or mechanical constraints, the transformers for CEET applications usually have a relatively large separation between the primary and secondary windings. Therefore, the characteristics of these transformers are very different from those of the conventional transformers that have good coupling between the windings.

Due to a large winding separation, the transformers for CEET applications have a relatively large leakage inductance, as well as increased proximity-effect winding losses. Furthermore, for the CEET transformers where the primary and secondary winding are wound on two magnetic pieces separated by an air gap, the magnetizing inductance is significantly reduced. This reduced magnetizing inductance increases the conduction losses because of an increased magnetizing current. In addition, due to a strong radiation from the gap, the transformers with a large air gap require a special attention to meet EMC requirements. To alleviate problems associated with the energy stored in a relatively large leakage inductance of a CEET transformer such as a reduced efficiency and increased component stress, converter topologies which incorporate the leakage inductance into the circuit operation such as resonant and soft-switched topologies are the optimal choice in CEET applications.

A typical CEET system consists of a transmitter, a CEET transformer, and a receiver, as shown in Fig. 1. The transmitter function is to generate an ac signal that is transferred to the receiver through the transformer. The transmitted signal is then conditioned by the receiver to provide the desire signal to the load. Generally, output voltage V_O of the CEET can be either a dc or an ac voltage. Similarly, the input to the CEET system can be either a dc voltage, as shown in Fig. 1, or an ac voltage. For the ac input, voltage V_S applied to the input of the transmitter is the rectified input voltage.

With no connections between the input side and output side, the control and protection of the CEET converters is very much different than the control of the converters that employ a conventional feedback control that uses signal communication between the output and input. Moreover, in CEET applications with a wide input-voltage and load range that require a tight regulation of the output such, for example,
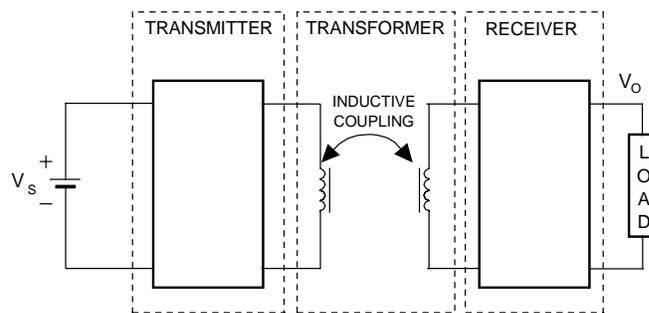

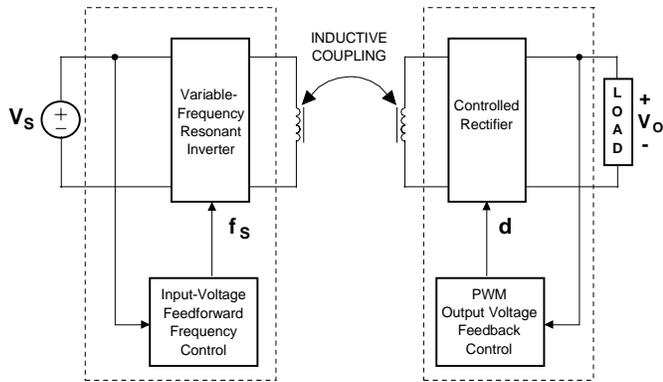Fig. 1. Block diagram of CEET system with dc (battery) input.

Fig. 2. Block diagram of CEET system.

in universal-line (90 – 264 V_{ac}) chargers for portable telephones, control design requires a unique approach.

Various aspects of inductive CEET have been addressed in a number of papers and patents. For example, mechanical design issues related to CEET systems were discussed in [1], [3] – [10], where a number of mechanical structures for CEET systems were proposed. The common goal of all these articles and patents is to define a reliable, easy-to-use mechanical structure which can provide consistent characteristics of the CEET transformer so that the conversion efficiency and EMC performance can be optimized.

Some limited topological and control issues were presented in [1], [3], and [8]-[10]. In [1] and [3], inductive coupling was implemented at a high-frequency by employing an inverter on the input side to convert the source signal into a high-frequency signal that is coupled to the output rectifier circuit through a CEET transformer. In addition, [1] proposes a method for maximizing the transmitted power by the input-side control that employs a phase-locked loop. In [8], a line-frequency inductive-coupling scheme and output voltage control using a saturable output-side inductor are described. Generally, a line-frequency CEET suffers from a significantly larger size and weight compared to its high-frequency counterpart.

In this paper, a high-frequency, high-efficiency, fully-regulated CEET system suitable for applications with a wide input range and wide load range is described. The CEET system consists of an input-side high-frequency resonant inverter and an output-side locally-regulated rectifier that are used to transmit and regulate power through a transformer. The high efficiency of the system is achieved by recovering the energy stored in the leakage inductances of the transformer by incorporating them in the operation of the circuit, and by employing high-frequency-inverter and a controlled-rectifier topologies that allow for bi-directional power flow through the transformer. With the ability of the system to transfer power through the transformer in both directions, i.e., from the primary to the secondary side, and

vice verse, the energy stored in the leakage inductances can be either transferred to the output, or to the input, depending on the load requirement.

The output regulation of the proposed CEET system with respect to the input and load changes is performed by a dual modulation. A local variable-frequency modulation is used on the input side to maintain an approximately constant power transfer for a varying input, whereas a local PWM modulation on the output side is primarily used to tightly regulate the output against the load changes. The variable-frequency modulation is implemented with feedforward control, i.e., by changing the inverter's frequency as a function of the input voltage.

Finally, the performance evaluation results of the proposed CEET system were presented using a 4.5-W, universal-line-range (90-265 V_{rms}) battery-charger prototype for portable telephones.

2. Analysis of Operation

A block diagram of the proposed CEET system is shown in Fig. 2. The system consists of a variable-frequency (VF) resonant inverter at the input side and a controlled bi-directional rectifier at the output side that are inductively coupled trough a transformer. The input voltage to the inverter is sensed and the sensed voltage is used to control the switching frequency of the inverter so that the transferred power through the transformer is maintained approximately constant with the input voltage changes. Generally, this frequency modulation scheme may be nonlinear. The bi-directional rectifier at the output side is controlled by a PWM control to maintain a tight regulation of the output voltage in the presence of a varying load, as well as to provide, if necessary, additional regulation against the input voltage changes not rejected by the variable-frequency control of the input-side inverter.

To maximize the conversion efficiency by recovering the energy stored in relatively large inductances of the CEET
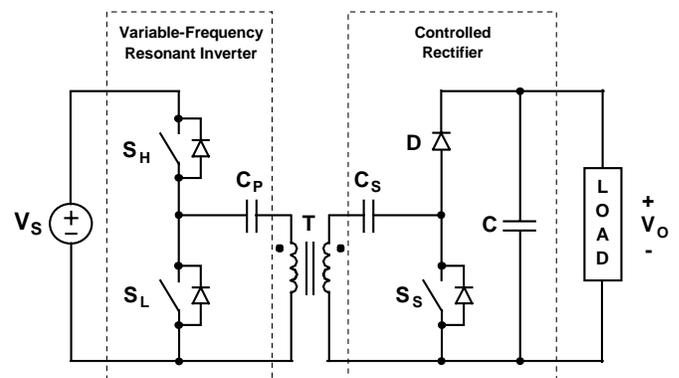

Fig. 3. Schematic diagram of inductive-coupled power stage with series-resonant inverter and controlled rectifier.

transformer, the variable-frequency inverter needs to be implemented with a resonant topology. Generally, any resonant topology can be employed. Moreover, the resonant inverter can be operated below or above the resonant frequency depending on the application. If operated above the resonant frequency, the inverter switches are turned on at zero voltage, which is preferred in applications with a high input voltage. If the inverter is operated below the resonant frequency, the inverter switches are turned off at zero current, which is advantageous in high-current applications, and/or when IGBTs (Insulated-Gate Bipolar Transistors) are used for the switches.

As an example, Fig. 3 shows the implementation of the CEET system with a series resonant inverter. To facilitate the analysis of the circuit, Fig. 4 shows the circuit in Fig. 3 with the leakage and magnetizing inductances of the transformer explicitly shown. Also, in Fig. 4 the load is replaced by a voltage source because it is assumed that the constant output voltage has a negligible ripple. The series resonant circuit in Fig. 4 is formed by capacitors C_P and C_S, and leakage inductances L_P and L_S. The approximate resonant frequency of the resonant circuit is given by

$$\omega_0 = \frac{1}{\sqrt{(L_P + n^2 L_S) \cdot (C_P + C_S/n^2)}}, \qquad (1)$$

where $n=N_P/N_S$ is the turns ratio of the transformer.

To further facilitate the explanation of the operation, Fig. 5 shows topological stages of the circuit in Fig. 4 during a switching cycle, whereas Fig. 6 shows the power-stage key waveforms for operation above the resonant frequency.

The following analysis of operation of the circuit in Fig. 4 assumes that all semiconductor components in the circuit are ideal, i.e., that they exhibit zero resistance when in the on state and infinite resistance in the off state. However, the capacitances of the switches are not neglected in this analysis. Finally, to further simplify the analysis, it is assumed that the magnetizing current i_M in Fig. 4 is in phase with resonant current i_{LS}. Generally, magnetizing current i_M is lagging
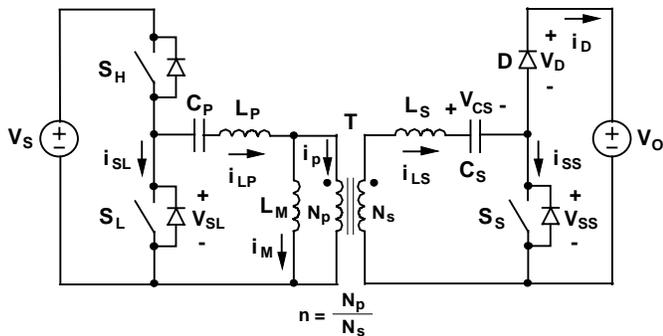

Fig. 4. Detailed schematic block diagram of power stage in Fig. 3 that shows leakage and magnetizing inductances of transformer T, and reference directions of currents and voltages.

resonant current i_{LS}, and the amount of the phase lag is a function of the load. Nevertheless, this assumption does not have any significant effect on the explanation of the principle of operation of the proposed circuit.

Before low-side switch S_L is turned off at $t=T_0$, negative primary-side resonant current $i_{LP} = i_M + i_P = i_M + i_{LS}/n$ flows through leakage inductance L_P, resonant capacitor C_P, and low-side switch S_L, whereas, negative secondary-side resonant current i_{LS} flows through leakage inductance L_S, resonant capacitor C_S, and the antiparallel diode of secondary switch S_S, as shown in Fig. 5(j). At the same time, diode D is off blocking output voltage V_O, whereas, high-side switch S_H is off blocking input voltage V_S.

After switch S_L is turned off at $t=T_0$, resonant current i_{LP} flowing through switch S_L is diverted from the switch to its output capacitance C_{OSSL}, as shown in Fig. 5(a). As a result, the voltage across S_L starts increasing, whereas the voltage across high-side switch S_H starts decreasing, as illustrated in Fig. 6, since the sum of the voltages across S_L and S_H is equal to source voltage V_S. When the voltage across S_L reaches zero at $t=T_1$, i.e., when output capacitance of high-side switch C_{OSSH} is fully discharged, the antiparallel diode of switch S_H begins to conduct, as shown in Fig. 5(b). At the same time, low-side switch S_L is off blocking input voltage V_S. Because after $t=T_1$ source voltage V_S is connected to the resonant circuit, the resonant current starts increasing. This topological stage ends at $t=T_3$ when i_{LP} reaches zero and the antiparallel diode of S_H stops conducting. As can be seen from Fig. 6, to achieve zero-voltage switching (ZVS) of S_H, it is necessary to turn on S_H before $t=T_3$, i.e., S_H should be turned on while its antiparallel diode is conducting. In Fig. 6, S_H is turned on at $t=T_2$ with ZVS. After $t=T_3$, current i_{LP} continues to flow through closed switch S_H, as shown in Fig. 5(d). Because of the assumption that currents i_M and i_{LS} are in phase, when direction of i_{LP} is reversed at $t=T_3$, the direction of i_M and i_{LS} is also reversed, as illustrated in Fig. 6. Consequently, at $t=T_3$, current i_{LS} which was flowing through the antiparallel diode of S_S is diverted to rectifier diode D. This topological stage ends at $t=T_4$, when secondary switch S_S is turned on. As shown in Fig. 5(e), after S_S is turned on, resonant current i_{LS} is commutated from rectifier D switch S_S. This topological stage ends at $t=T_5$, when switches S_H is turned off. After switch S_H is turned off at $t=T_5$, resonant current i_{LP} flowing through switch S_H is diverted from the switch to its output capacitance C_{OSSH}, as shown in Fig. 5(f). As a result, after $t=T_5$, C_{OSSH} is being charged, while C_{OSSL} is being discharge. When C_{OSSL} is fully discharged at $t=T_6$, the antiparallel diode of switch S_L begins to conduct, as shown in Fig. 5(g). At the same time, high-side switch S_H is off blocking source voltage V_S. This topological stage ends at $t=T_8$, when i_{LP} reaches zero, as shown in Fig. 5(h). As can be seen from Fig. 6, to achieve ZVS of S_L, it is necessary to turn on S_L before $t=T_8$, i.e., S_L should be turned on while the antiparallel diode of S_L is conducting. In Fig. 6, S_L is turned on at $t=T_7$ with ZVS. As shown in Figs. 5(i) and 6, after $t=T_8$, the direction of currents
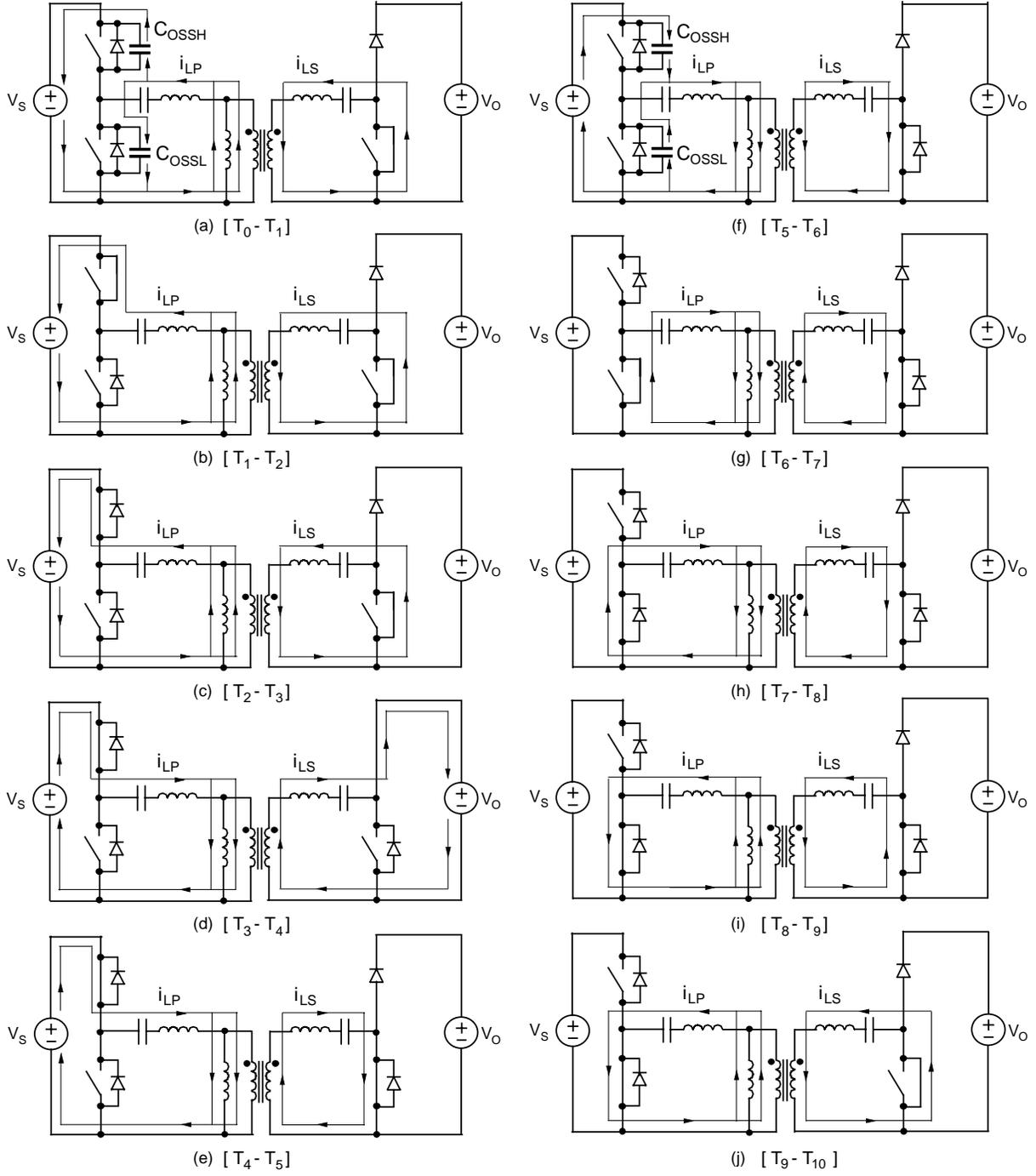
Fig. 5. Topological stages of power stage in Fig. 4 during switching cycle.

i_{LP}, i_M, and i_{LS} is reversed so that current i_{LP} flows through S_L, whereas, current i_{LS} flows through S_S. This topological stage ends at $t=T_9$, when secondary switch S_S is turned off and current i_{LS} flowing through S_S is commutated to the antiparallel diode of S_S, as shown in Fig. 5(j). The circuit stays in this topological stage until the next switching cycle is initiated at $t=T_{10}$.

As can be seen from Fig. 6, the voltage stress of switches S_H and S_L is limited to source voltage V_S, while the voltage stress of switch S_S and output rectifier D is limited to output
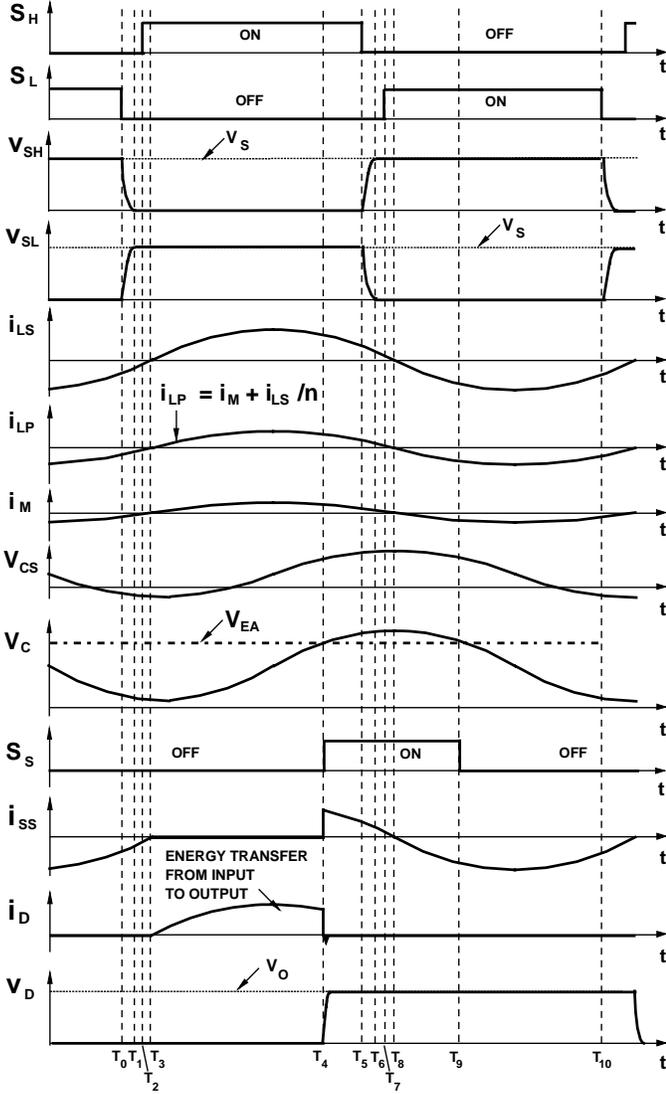
Fig. 6. Key waveforms of power stage in Fig. 5.

voltage V_O. Also, from the i_D waveform in Fig. 6 can be seen that in the circuit in Fig. 4 the energy is transferred from the input to the output only during the conduction of secondary-side rectifier D, i.e., during the time interval from $t=T_3$ to $t=T_4$. Generally, this time interval represents the time from the moment current i_{LS} becomes positive at $t=T_3$ to the time secondary-side switch S_S is turned off at $t=T_4$. Therefore, the output of the proposed converter can be regulated by varying the duration of the T_3-T_4 interval by controlling the turn-on instant of S_S.

3. Design Guidelines

In the proposed CEET system, the secondary-side (rectifier) control is used primarily to regulate the output against the load changes. The regulation against the input voltage changes is implemented with a primary-side (inverter)

control. However, since the primary-side control cannot tightly regulate the output on the secondary side, the secondary-side control is also used to assist in regulation against the input voltage changes.

An implementation of the proposed CEET system is shown in Fig. 7. The inverter control in Fig. 7 is implemented by sensing input voltage V_S with a variable-gain input-voltage sensing circuit, and by changing frequency f_S of the voltage-controlled-oscillator (VCO) so that the inverter maintains approximately constant output power in the presence of input changes. Generally, for the operation above resonance, which offers ZVS, the frequency needs to be increased as the input voltage increases. The operation below resonance that offers zero-current switching (ZCS) requires that the frequency be reduced as the input voltage increases. In either case, the required change of the frequency is a nonlinear function of the input.

The output voltage control in Fig. 7 is implemented with a PWM modulation of the rectifier. In this control, sensed output voltage $V_{O(SENSE)}$ is compared with reference voltage V_{REF} at the input of the error amplifier. The generated error signal at the output of error amplifier V_{EA} is then compared with signal V_C that is proportional to instantaneous secondary current i_{LS}. In the implementation in Fig. 7, the secondary-side current information is obtained indirectly, i.e., without the use of a sensing transformer or a resistor. The indirect current sensing is implemented by a differential sensing of voltage V_{CS} across capacitor C_S, and by a subsequent scaling and level shifting of the sensed voltage so that the minimums of the scaled voltage correspond to the zero crossings of secondary current i_{LS}, as can be seen from Fig. 6.

It should be noted that since secondary switch S_S is turned on with a minimum duty cycle at full load, the time interval between $t=T_3$ and $t=T_4$ at full load is approximately a half of a switching cycle, i.e., the entire positive resonant current flows
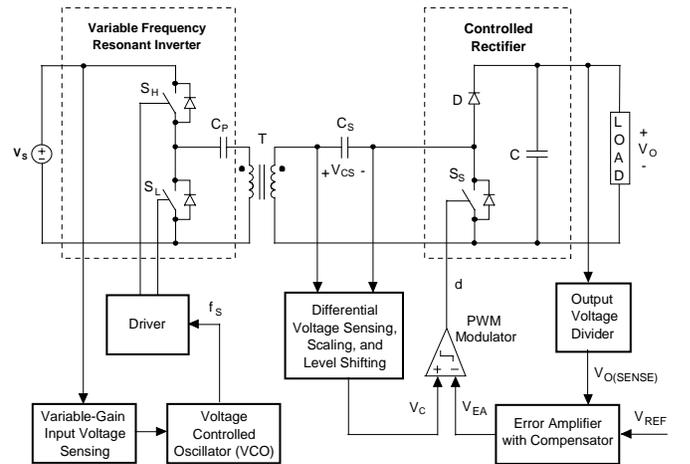

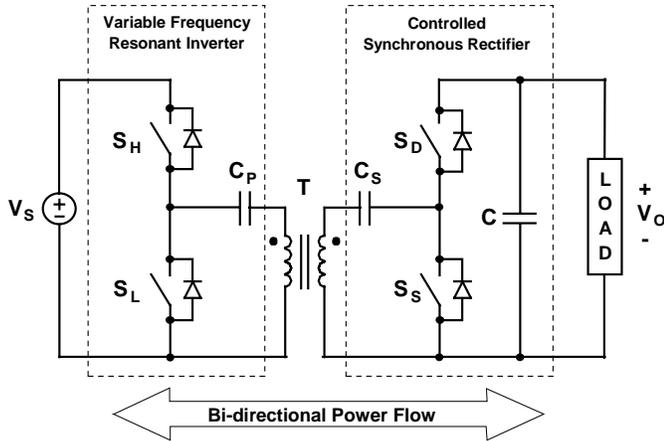Fig. 7. Block diagram of control for power stage in Fig. 4.

Fig. 8. Schematic circuit diagram of power stage with bi-directional rectifier.

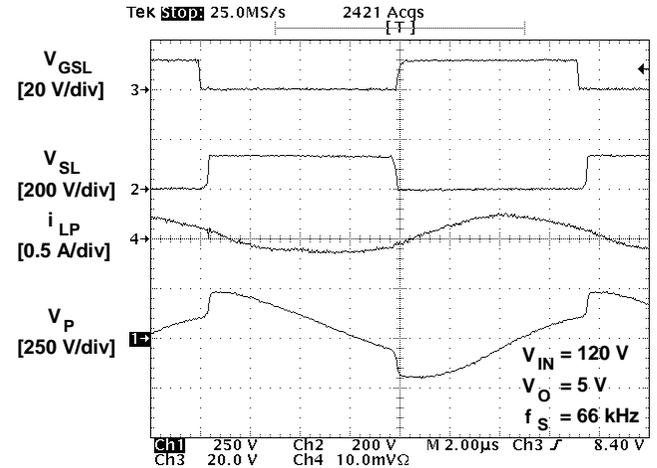

Fig. 9. Measured key waveforms of experimental converter at V_S=120 V and P_O=4.4 W. Time base: 2 µs/div.

Fig. 10. Measured key waveforms of experimental converter at V_S=376 V and P_O=4.4 W. Time base: 2 µs/div.

to the load. On the other hand, at no load, secondary switch S_S turns on with a maximum duty cycle so that the interval between t=T_3 and t=T_4 is zero, whereas, the time interval between t=T_4 and t=T_5 becomes a half of a switching cycle. Since without a load (or, at light loads) the resonant circuit is essentially undamped, primary resonant current i_{LP} is significantly increased at no load. Generally, this increase of i_{LP} at no load requires a protection circuit to ensure that the converter safely operates at no load. One approach to overcome the no-load problem is to detect the no-load condition, and to change the frequency of the inverter so that the power transfer through the inverter is reduced. This can be accomplished by rising the switching frequency if the inverter operates above resonance, or by reducing the switching frequency if the inverter operates below the resonant frequency. Another approach is to implement overcurrent protection with automatic restart, i.e., to turn off inverter switches S_H and S_L for a pre-set period of time and then restarts the inverter. By operating the circuit in this "burst", or "hiccup" mode, the light load efficiency can be maximized.

Finally, in low output-voltage applications, the conversion efficiency of the CEET system in Fig. 4, can be improved by replacing rectifier D with a synchronous rectifier (SR), as shown in Fig. 8. Furthermore, the implementation in Fig. 8 allows bi-directional flow from the source to the load, and vice-verse, because both the inverter and the rectifier can conduct current in both directions.

4. Experimental Results

The performance of the proposed CEET system was evaluated on a 4.5 W (5 V/ 0.9 A), universal-line-range (90 - 265 V_{ac}) battery charger for portable telephones. The experimental circuit was implemented using the IRF840 MOSFETS for primary switches S_H and S_L, and the IRF7421D1 for secondary switches S_S and S_D. The transformer was built using Philips 2624Z ferrite cores with the primary winding having 210 turns of AWG#31 magnet wire and the secondary winding having 9 turns of AWG#26 magnet wire. The separation (air gap) between the primary side magnetic piece and the secondary side magnetic piece of the transformer was approximately 60 mils. The output voltage of the experimental charger was regulated with a voltage ripple less than 2% over the entire input-voltage range.
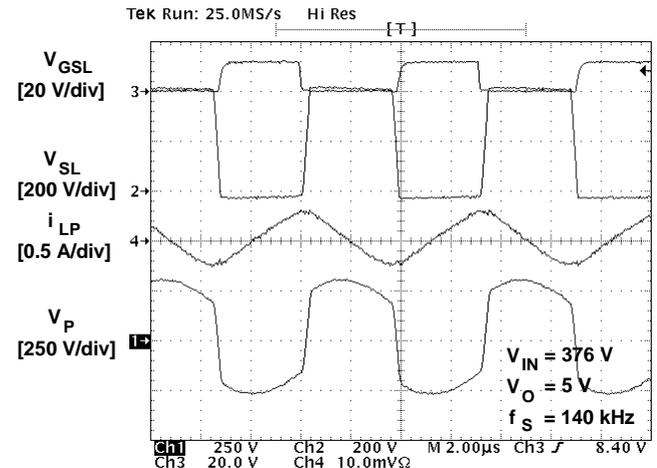
Figures 9 and 10 show the oscillograms of key waveforms of the experimental prototype for the minimum and maximum rectified input voltage. Figure 9 shows the measured waveforms of gate-source voltage V_{GSL} and drain-source voltage V_{SL} of primary switch S_L, primary resonant current i_P, and voltage V_P across the primary winding of transformer T at

rectified input voltage V_S = 120 V. Figure 10 shows the measured waveforms at rectified input voltage V_S = 376 V. The frequency range of the experimental circuit was from 65 kHz to 140 kHz. The measured efficiency (excluding the rectifier loss) was approximately 60-70% at full load over the entire input voltage range as summarized in Table I.

It should be noted that the major loss in the experimental circuit was the winding loss of the transformer due to a pronounced proximity effect brought about by the separation of the primary-side and secondary-side core halves. Generally, with a CEET transformer design that minimizes the proximity effect loss, a significantly higher efficiency can be achieved. However, in the experimental circuit reported in this paper no attempt was made to minimize this loss since the primary objective of the experimental circuit was to prove the proposed concept.

TABLE I

Efficiency Measurements

V_S [V]	I_{IN} [mA]	V_O [V]	I_O [mA]	η [%]	f_S [kHz]
120	53.0	5.05	870	69.2	66
157	38.7	5.0	859	70.8	75
181	33.8	5.04	866	71.4	90
204	31.1	5.08	875	69.9	98
318	21.2	5.01	856	63.6	130
363	19.8	5.02	861	60.1	138
376	19.5	5.03	865	59.4	140

5. Summary

A high-frequency, high-efficiency, fully-regulated CEET system suitable for applications with a wide input and load range has been described. The proposed CEET system consists of an input-side, variable-frequency resonant inverter and an output-side locally-regulated rectifier. A high-efficiency of the system is achieved by recovering the energy stored in the leakage inductances of the transformer by incorporating them in the operation of the circuit, and by employing high-frequency-inverter and controlled-rectifier topologies that allow a controlled bi-directional power flow through the transformer. In addition, a feedforward variable-switching-frequency control of the inverter is used to maintain approximately constant power transfer through the transformer with the input voltage changes, whereas, the output-side rectifier employs a local PWM control to achieve a tight regulation of the output in the presence of load variations. The proposed CEET system was experimentally verified on a 4.5-W prototype battery charger for portable telephones.

References

[1] D.A.G. Pedder, A.D. Brown, and J.A. Skinner, "A Contactless Electrical Energy Transmission System,", *IEEE Trans. Industrial Electronics*, vol. 46, no. 1, pp. 23 – 30, Feb. 1999

[2] A. Ghahary and B.H. Cho, "Design of Transcutaneous Energy Transmission System Using a Series Resonant Converter," *IEEE Power Electronics Specialist's Conf. Record*, 1990, pp. 1 – 8.

[3] E. Dahl, *Induction Charging System,* U.S. Pat. 3,938,018, Feb. 10, 1976.

[4] N. Ishi, T. Ina, K. Mori, K. Ito, and S. Asai, *Electric Power Transmitting Device with Inductive Coupling,* U.S. Pat. 5,070,293, Dec. 3, 1991.

[5] P. Carosa, *Separable Inductive Coupler*, U.S. Pat. 5,216,402, Jun. 1, 1993.

[6] K. Klontz, D. Divan, D. Novotny, and R. Lorenz, *Contactless Battery Charging System,* U.S. Pat. 5,341,083, Aug. 23, 1994.

[7] I. Shirai, H. Yamagami, E. Hiroshige, and K. Kubo, *Induction Charging Apparatus,* U.S. Pat. 5,550,452, Aug. 27, 1996.

[8] J. Bolger and L. Ng, *Inductive Power Coupling with Constant Voltage Output,* U.S. Pat. 4,800,328, Jan. 24, 1989.

[9] C. G. Kim, D. H. Seo, J. S. You, J. H. Park, and B.H. Cho, "Design of a Contactless Battery Charger for Cellular Phone," *IEEE APEC Record*, 2000, pp. 769 – 773.

[10] Y. Kanai, M. Mino, T. Sakai, and T. Yachi, "A Non-Contact Power-Supply Card Powered by Solar Cells for Mobile Communications," *IEEE APEC Record*, 2000, pp. 1157 – 1162.